# Optimization of Mn doping in group-IV-based dilute magnetic semiconductors by electronic codopants

Hua Chen and Wenguang Zhu
*Department of Physics and Astronomy, University of Tennessee, Knoxville, Tennessee 37996, USA*
*and Materials Science and Technology Division, Oak Ridge National Laboratory, Oak Ridge, Tennessee 37831, USA*

Efthimios Kaxiras
*Department of Physics and School of Engineering and Applied Sciences, Harvard University, Cambridge, Massachusetts 02138, USA*

Zhenyu Zhang
*Materials Science and Technology Division, Oak Ridge National Laboratory, Oak Ridge, Tennessee 37831, USA*
*and Department of Physics and Astronomy, University of Tennessee, Knoxville, Tennessee 37996, USA*
(Received 18 February 2009; revised manuscript received 6 May 2009; published 4 June 2009)

The percentage of substitutional doping of magnetic atoms (Mn) in group-IV-based dilute magnetic semiconductors can be increased by codoping with another conventional electronic dopant, as demonstrated from first-principles calculations recently [W. G. Zhu, Z. Y. Zhang, and E. Kaxiras, Phys. Rev. Lett. **100**, 027205 (2008)]. Here, we report extensive theoretical investigations of the kinetic and thermodynamic characteristics of several codoped systems including bulk Si and Ge as hosts and various group-III and group-V dopants. The main findings are as follows. The *n*-*p* pairing of *n*-type codopants with *p*-type substitutional Mn is energetically stable in bulk Ge and Si. Mn atoms move from interstitial sites to substitutional sites easier (with lower kinetic barriers) in the presence of a neighboring *n*-type codopant. Magnetic coupling between two Mn atoms in bulk Ge oscillates between positive (ferromagnetic) and negative (antiferromagnetic) values with increasing Mn-Mn distance, but in Mn/As codoped Ge the coupling parameter remains positive at all distances beyond nearest neighbors and this qualitative difference does not change with the doping level. For Mn-doped Si, all coupling values except for the nearest-neighbor one are positive and do not change much upon codoping. We find an unconventional magnetic anisotropy in the codoped system, that is, the dependence of magnetic coupling on the relative positions of the magnetic ions and their neighboring donors. We map the calculated magnetic coupling to a classical Heisenberg model and employ Monte Carlo simulations to estimate the Curie temperature ($T_c$). We find that in Mn-doped Ge no ferromagnetic order exists for Mn concentrations ranging from 3.13% to 6%. Instead, a spin-glass phase transition occurs at ~5 K at 5% Mn doping. For Mn/As codoped Ge, $T_c$ increases nearly linearly with the Mn concentration and reaches 264 K at 5% Mn doping.

DOI: 10.1103/PhysRevB.79.235202 PACS number(s): 75.50.Pp, 66.30.J−, 75.30.Hx, 87.10.Rt

## I. INTRODUCTION

Dilute magnetic semiconductors (DMSs) have attracted much interest in the condensed-matter community not only because of their promising application in the spintronic devices[1,2] but also because of the many new and important theoretical issues which arise from the study of this unique class of disordered magnetic system.[3–7] As for specific materials, besides the most extensively studied (III,Mn)V systems,[6,8] Mn-doped group-IV semiconductors such as Ge and Si also show promise for real applications.[9–15] In order to realize this promise, a Curie temperature comparable to room temperature or higher is required. Both theory and experiment indicate that the Curie temperature of the above-mentioned materials is exceptionally sensitive to the ratio of interstitial to substitutional Mn atoms.[7,16–19] In (III,Mn)V as well as (Mn,IV) systems, substitutional Mn atoms act as acceptors and provide holes which, according to current understanding, are the mediator of magnetic interactions between magnetic moments in these materials. Interstitial Mn atoms[19] are identified to be donors and tend to compensate the holes and magnetic moments induced by the substitutional Mn.[6] Furthermore, though annealing is an effective way to decrease the percentage of interstitial Mn while keeping the homogeneity in (Ga,Mn)As,[20,21] it is less useful for $Mn_xGe_{1-x}$ and $Mn_xSi_{1-x}$,[22–25] which makes it very difficult to get high-quality samples of these materials using conventional methods.

In our recent work,[26] a novel way to enhance the substitutional doping of Mn in Ge and Si was proposed. In this method, an additional conventional electronic dopant such as As or P is introduced in the doping process. Using first-principles electronic structure calculations, we were able to show that the codoping approach can substantially lower the energy of Mn atoms at substitutional sites relative to that at interstitial sites, as well as the energy barrier which the Mn atoms have to overcome in order to be incorporated into substitutional sites. In addition, the codopant enhances the magnetic coupling between substitutional Mn atoms. A different type of magnetic anisotropy was also found, which depends on the proximity of the codopant to a Mn dopant, rather than the direction of magnetic moments relative to the lattice direction of the host or to other moments.

In this paper, we present a detailed *ab initio* investigation

 

of this approach by analyzing the kinetic and thermodynamic issues related to the stability of various dopant-host combinations. We then calculate the magnetic coupling between two Mn atoms in bulk Ge and Si and find that in Ge, the coupling oscillates between positive (ferromagnetic) and negative (antiferromagnetic) values with the Mn-Mn distance. But in Mn/As codoped Ge the coupling parameter remains positive at all distances beyond nearest neighbors, and this qualitative difference does not change with the doping level. For Mn-doped Si, all the couplings except for the nearest-neighbor one are positive and do not change much upon codoping. We also carry out Monte Carlo (MC) simulations to obtain the Curie temperatures of the codoped materials. We find that in Mn-doped Ge no ferromagnetic order exists for Mn concentrations ranging from 3.13% to 6%. Instead, a spin-glass phase transition occurs at ~5 K at 5% Mn doping. For Mn/As codoped Ge, $T_c$ increases nearly linearly with the Mn concentration and reaches 264 K at 5% Mn doping.

The paper is organized as follows. In Sec. II we present the computational methodology, including details of our *ab initio* treatment and the Monte Carlo simulations. The main *ab initio* results are given in Sec. III where the kinetic and energetic properties of various combinations of host materials (Ge and Si) and codopants (As, P, Al, and Ga) are investigated. Magnetic interactions in As codoped $Mn_xGe_{1-x}$ are discussed in Sec. IV. In Sec. V the *ab initio* results of magnetic coupling are used to find the transition temperature $T_c$ of Mn/As codoped Ge. The discussion and summary are provided in the last two sections.

## II. METHODS

Our spin-polarized first-principles calculations are carried out using the Vienna *ab initio* simulation package (VASP),[27] a density-functional theory (DFT) approach using the projector augmented wave (PAW) method,[28,29] and the Perdew-Burke-Ernzerhof version of the generalized gradient approximation (PBE-GGA) (Ref. 30) for exchange correlation. A default plane-wave energy cutoff of 269.9 eV is consistently used in all Mn calculations. These choices produce a bulk Ge and Si lattice constants of 5.78 Å (experimental value[31] of 5.66 Å) and 5.47 Å (experimental value[32] of 5.43 Å), respectively.

In our calculations of the codoping process the supercell size is chosen to be a $2\times2\times2$ multiple of the conventional cubic cell of the diamond lattice which contains 8 atoms. Hence, there are 64 atoms in one supercell, and one of them is replaced by an Mn atom, corresponding to 1.563% Mn concentration, comparable to what was achieved experimentally.[9,33,34] Different supercell sizes were used to study the dependence of calculated results on Mn concentration. Specifically, we used a $3\times3\times3$ supercell, which corresponds to 216 atoms, and with one of them replaced by a Mn the concentration is 0.463%. In each calculation of the magnetic coupling between Mn atoms, two Mn atoms are placed in a $3\times3\times3$ supercell, corresponding to a 0.926% Mn concentration. We also selectively use a $2\times2\times2$ supercell for the magnetic coupling with two Mn atoms in the supercell, corresponding to 3.125% Mn, for comparison. This setup is similar to previous studies of Mn-Mn interactions in pure semiconductors.[35–38]

A uniform $4\times4\times4$ $(2\times2\times2)$ mesh, including the Γ point (0, 0, 0), is chosen for Brillouin zone sampling in the $2\times2\times2$ $(3\times3\times3)$ supercell. Optimized atomic geometries are obtained when the forces on all the unconstrained atoms are smaller in magnitude than 0.01 eV/Å. The "climbing image nudged elastic band" (NEB) method[39] is used to locate the transition state geometries for the calculation of activation energy barriers. Typically four slab replicas between the initial and final geometries are enough to produce a smooth minimum-energy path.

For the Monte Carlo simulations we use the Metropolis algorithm[40] and the magnetic energy of the system is calculated using the classical Heisenberg model, in which each magnetic ion is treated as a classical moment and is placed at a randomly chosen site of the supercell. The magnetic coupling parameters are extracted from *ab initio* results of the energy difference between parallel and antiparallel spin configurations of two Mn moments at different separations. At each temperature we use 50 000 Monte Carlo steps per moment for the system to relax and calculate the thermal average in the following 50 000 steps. To determine the Curie temperature, we adopt the fourth order cumulant crossing method based on the finite-size scaling theory proposed by Binder.[40,41] In applying this method we choose three supercell sizes, $8\times8\times8$, $10\times10\times10$, and $12\times12\times12$, and 40 configurations in each case for averaging.

## III. *AB INITIO* STUDY OF THE CODOPING PROCESSES

### A. Study on intrinsic (Mn,IV) without codopants

We first consider the equilibrium structure of a single Mn dopant atom in bulk Si and Ge, and address the difficulty of lowering the percentage of interstitial Mn impurities. A complete understanding of the microscopic doping process requires detailed knowledge of the energetics as well as the kinetics of dopants in the host material.[16] In fact, an in-depth understanding of the growth kinetics is particularly important because the DMS systems are typically in a metastable state, since they are grown by codoping the magnetic dopants and the host semiconductor atoms using molecular-beam epitaxy under nonequilibrium conditions.[9,33,42,43]

To address these issues, we calculate the relative formation energy of a substitutional Mn [Fig. 1(a)] and interstitial Mn [Fig. 1(b)] atom in Ge and Si separately, which is defined as

$$\Delta E_1 = (E_{\text{subst}} + \mu_{\text{host}}) - E_{\text{inter}}, \tag{1}$$

where $\mu_{\text{host}}$ is the host material's chemical potential. For Ge, our calculation gives $\Delta E_1 = -0.63$ eV. Thus, in Ge the substitutional sites have a relatively lower energy and are preferred by Mn atoms. However, for Si the opposite is true and $\Delta E_1 = +0.58$. This reversed site preference[44] makes it extremely hard to achieve experimentally even a nominal concentration of substitutional Mn in silicon.

We next consider kinetic aspects of the Mn doping process. In order to get a high ratio of substitutional to interstitial Mn, the process that an interstitial Mn kicks out a host

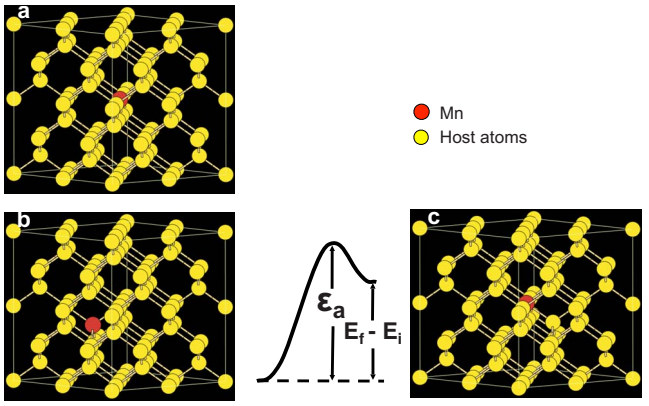


FIG. 1. (Color online) Different Mn sites in bulk Si or Ge: (a) Mn at a substitutional site. (b) Mn at an interstitial site. (c) Final state of an interstitial Mn kicking out a neighboring host atom to an interstitial site and occupying the left-behind substitutional one.

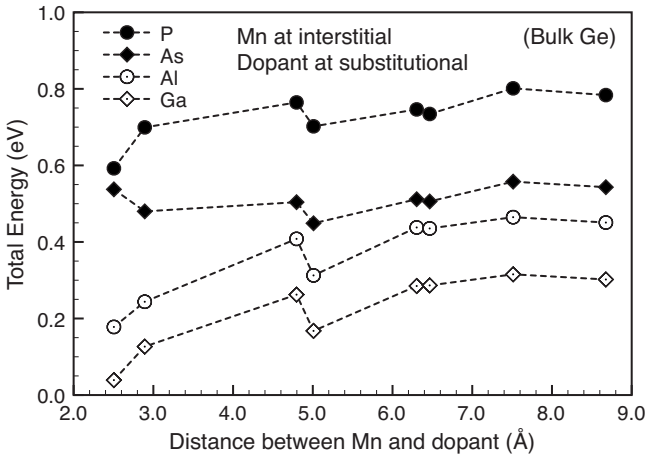


FIG. 2. Calculated relative total energy as a function of the distance between an interstitial Mn and a substitutional codopant in bulk Ge.

atom and becomes substitutional must take place more often than the reverse process. Accordingly, we calculate the energy difference between the initial [interstitial, Fig. 1(b)] and final [substitutional, Fig. 1(c)] states of this process, $\Delta E = E_f - E_i$, and the energy barriers $\varepsilon_a$ and $\varepsilon_a'$ for the reverse process. Our calculation shows that for both Ge and Si $\Delta E$ is positive (0.82 and 2.03 eV, respectively). This energy cost for the transition from initial to final state defines the lower bound of the activation energy barrier for the exchange process, which must be lower than ~0.8 eV for efficient incorporation (with a standard attempt frequency $10^{12}$ $s^{-1}$). Moreover, the actual energy barrier $\varepsilon_a$ in either case (1.12 eV for Ge and >2 eV for Si) is higher than the barrier of the reverse process, which is calculated as $\varepsilon_a' = \varepsilon_a - \Delta E$, with the latter being lower than 0.8 eV, further facilitating the reverse processes. Thus, kinetically Mn is more stable at interstitial sites rather than at substitutional sites in both Ge or Si. In the following section we will address the issue of doping Mn together with another *n*- (P, As) or *p*-type (Al, Ga) conventional electronic dopant in order to explore how the codopants influence this site preference both energetically and kinetically.

### B. Energetic and kinetic study on the codoped systems

Substitutional Mn in Ge is a *p*-type double acceptor.[45] Our proposal for a codoping mechanism is based on the fact that the electrostatic interaction between an *n*-type and a *p*-type dopant in a semiconductor is attractive because of their different charge states (see below). Thus an *n*-type dopant may help to stabilize substitutional Mn atoms.

We start by noting that in Ge or Si there are two kinds of interstitial sites: the hexagonal interstitial site $I_H$, which has six nearest neighbors, and the tetrahedral site $I_T$ with four nearest neighbors. Using first-principles calculations we find that in *n*-type-doped Ge and Si, the energy of a Mn sitting at the $I_H$ site is different from that at the $I_T$ site. For P-, As-, and Sb-doped Ge, the energy differences are 0.14, 0.09, and 0.04 eV, respectively, where a positive sign means that the $I_H$ occupation has a lower energy and is preferred. In the case of either *n*- or *p*-doped Si as well as *p*-doped Ge, $I_T$ is preferred to $I_H$. This codopant-dependent preference can be qualitatively explained by the local strain effect. Namely, a Mn atom and an *n*-type codopant favor a relatively short bonding distance, which is accommodated by Mn occupying the $I_H$ site rather than the $I_T$ site in Ge (the $I_H$ site has a shorter distance to its nearest neighbors than the $I_T$ site). To show that this is indeed the case, we reduce the lattice constant of Ge to the value of Si and calculate the energy difference again. Then the results show that the preference for Mn is changed to the $I_T$ site, because in this case the distance between the $I_H$ Mn and *n*-type codopant becomes too short (compressive), whereas at the $I_T$ site the Mn/*n*-type codopant bond length is close to its optimal value. We have also checked to confirm that if we increase the lattice constant of Si to that of Ge, the preference for Mn is changed to the $I_H$ site for the *n*-type-doped systems.

In the following we examine two possible kinetic processes of an interstitial Mn atom becoming substitutional. These processes share the same initial state with Mn occupying either the $I_H$ or $I_T$ sites with a neighboring *n*-type or *p*-type codopant. From our calculation of the total energy of a Ge supercell with an interstitial Mn and a substitutional codopant as a function of their separation, shown in Fig. 2, we find that shorter separation is energetically preferred. Thus, the choice of neighboring Mn/codopant pair configuration is reasonable.

In the first process, denoted as process I, we consider an interstitial Mn directly exchanging position with its substitutional codopant neighbor. In the final state, the codopant is pushed to an adjacent interstitial site and the Mn atom moves into the substitutional site left behind, as shown in Fig. 3. Table I summarizes the calculated energy differences $\Delta E$ between the final and initial states for *n*-type and *p*-type codopants in Si and Ge. We find that only the P- or As-doped Ge (with $\Delta E = 0.33$ and 0.42 eV, respectively) can fulfill the requirement that $\Delta E < 0.8$ eV. However, further examination of the activation energy barriers for incorporation in these two cases gives $\varepsilon_a = 0.88$ and 0.98 eV, respectively, which means this process is unlikely to happen in both cases.

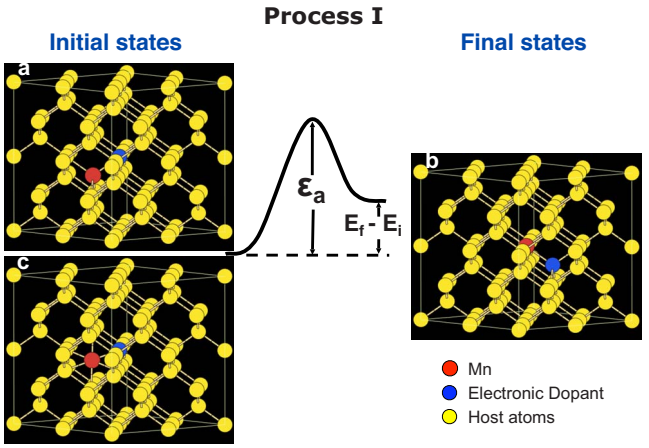


FIG. 3. (Color online) Atomic structures and schematic energy profiles for process I. (a) Initial state with Mn in the $I_T$ position (except for $n$-type-doped Ge). (b) Final state. (c) Initial state for $n$-type-doped Ge with Mn at the $I_H$ position.

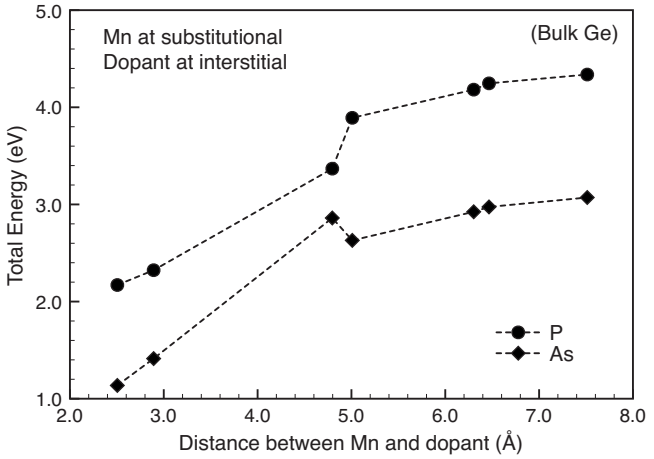


FIG. 4. Calculated relative total energy as a function of the distance between a substitutional Mn and an interstitial $n$-type codopant in bulk Ge.

Moreover, the reverse processes with $\varepsilon_a'$=0.55 and 0.56 eV, respectively, are more likely to occur.

Nevertheless, there is one possibility for the Mn atom to stay at the substitutional site, that is, the kicked-out codopant atom diffuses away rapidly so that the reverse process cannot happen. This is ruled out by our calculation of the energy of a Mn/codopant pair as a function of their separation, shown in Fig. 4, which shows that the codopant cannot diffuse away because the energy increases with increasing separation.

We then consider a different process (process II, shown in Fig. 5), which starts from the same initial configuration as in process I, but instead of exchanging with the codopant, the Mn atom now pushes out a host atom next to the codopant to an interstitial site, and then occupies the substitutional site left behind. The final state is shown in Fig. 5(b), in which the kicked-out interstitial host atom, the substitutional Mn and the codopant are nearly collinear. The calculated $\Delta E$ and $\varepsilon_a$ for various $n$-type and $p$-type codopants in Si and Ge are also shown in Table I. For $n$-type-doped Ge these values are substantially lower than in process I and considerably below the threshold value of 0.8 eV. For P- and As-doped Ge, $\Delta E$ is actually quite low. Furthermore, the activation barriers $\varepsilon_a$ for all the three $n$-type codopants are less than 0.4 eV. Qualitatively, this substantial change in the energetic and kinetic characters originates from the electrostatic attraction between the Mn atom, which behaves like a $p$-type dopant, and $n$-type codopants. Therefore, process II, leading to substitutional Mn atoms proximate to $n$-type codopants, is more likely to happen in reality.

One issue that arises at this stage is whether the final state is thermodynamically stable. To address this question, we calculate the energy difference between interstitial Mn and substitutional Mn defined as

$$\Delta E_2 = (E_{\text{pair}} + \mu_{\text{host}}) - E_{\text{inter}}. \tag{2}$$

Here $E_{\text{inter}}$ is the total energy of a Mn/codopant pair, with the Mn sitting at an interstitial site, while $E_{\text{pair}}$ is that with the Mn occupying a substitutional site. The calculated interstitial-substitutional energy difference $\Delta E_2$ is shown in Table II. Compared to the results without $n$-type codopants in Sec. III A, the substitutional Mn in Ge becomes much more stable with the neighboring $n$-type codopant. Moreover, the site preference of Mn in Si is reversed from interstitial to substitutional.

TABLE I. Calculated energy differences $\Delta E = E_f - E_i$ (in eV) between the final and initial states of process I and process II, illustrated in Figs. 3 and 5, respectively. $\varepsilon_a$ (in eV) is the activation energy for a transition from the initial to final state. Results highlighted in bold correspond to processes for which $\Delta E$ or $\varepsilon_a$ or both are $<0.8$ eV. All the results are for Mn concentration of 1.563%; results for selected cases with Mn concentration of 0.463% are given in brackets.

| Bulk Si | | | Bulk Ge | | | | |
|---|---|---|---|---|---|---|---|
| | $\Delta E = E_f - E_i$ | | | $\Delta E = E_f - E_i$ | | $\varepsilon_a$ | |
| $X$ | Process I | Process II | $X$ | Process I | Process II | Process I | Process II |
| Si | 2.03 | | Ge | 0.82[1.46] | | | |
| P | 1.46 | 0.89 | P | **0.33[0.59]** | **0.03[0.17]** | 0.88 | **0.34** |
| As | 1.55 | 1.09 | As | **0.42[0.66]** | **0.05[0.34]** | 0.98 | **0.25** |
| Al | 1.24 | 2.05 | Al | 0.94 | 1.54 | | |
| Ga | 1.79 | 2.43 | Ga | 1.05 | 1.52 | | |

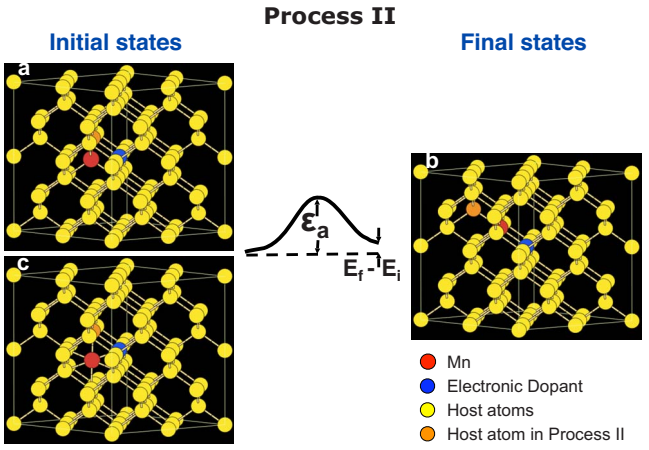


FIG. 5. (Color online) Atomic structures and schematic energy profiles of process II. (a) Initial state with Mn in the $I_T$ position (except for $n$-type-doped Ge). (b) Final state. (c) Initial state for $n$-type-doped Ge, with Mn at the $I_T$ position.

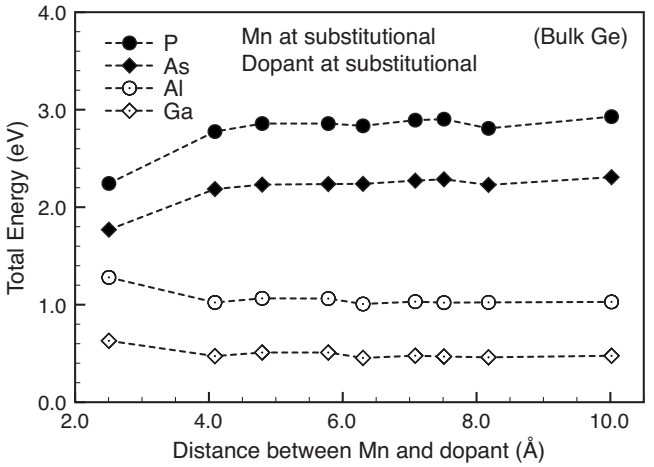


FIG. 6. Relative total energy as a function of the distance between a substitutional Mn and a substitutional codopant in bulk Ge.

We next calculate the total energy of a Ge supercell doped by a substitutional Mn/codopant pair at different separations. The trend of the total energy with increasing distance between the Mn atom and the codopant is shown in Fig. 6. The interaction between Mn and codopant is attractive for $n$-type codopants (P and As) and repulsive for $p$-type codopants (Al and Ga). This suggests that the picture of electrostatic interaction between Mn and codopants that we proposed at the beginning of this section is valid.

Finally we note that the energy differences between the initial and final states depend on the Mn concentration, as illustrated in Table I. The calculated $\Delta E$ values at the 0.46% Mn concentration are larger than those at the 1.56% concentration, but for the important cases of $n$-type codopants in Ge, these energy differences are still much lower than the threshold of ~0.8 eV. This relatively strong dependence is not due to constant volume calculations because it is also observed when the supercell volume is fully relaxed. Instead, it is caused by the interaction between the Mn atoms in adjacent supercells. We stress that the qualitative picture that the $n$-type codopants facilitate substitutional incorporation of Mn is valid for all the experimentally accessible Mn concentrations considered here.

In short, we have shown that in the presence of a neighboring $n$-type codopant, the substitutional sites are energetically preferred by Mn atoms to interstitial sites and are kinetically accessible. In the following sections we will turn to study the electronic and magnetic properties of this $n$-$p$ codoped system. From now on we will call the $n$-type electronic codopants directly by donors.

TABLE II. Relative formation energy of substitutional and interstitial Mn in the presence of a neighboring substitutional $n$-type codopant, defined as $\Delta E_2=(E_{\text{pair}}+\mu_{\text{host}})-E_{\text{inter}}$ (in eV). Negative values indicate higher stability of the substitutional configuration over the interstitial. The relative energy of substitutional and interstitial Mn in pure Si or Ge are included for comparison.

| | P | As | Undoped |
|---|---|---|---|
| Si | −0.84 | −0.87 | +0.58 |
| Ge | −1.35 | −1.42 | −0.63 |

## IV. ELECTRONIC AND MAGNETIC PROPERTIES OF THE CODOPED SYSTEMS

### A. Electronic structure

The electronic properties of the Mn/donor codoped systems are conveniently presented through the calculated density of states (DOS). Figures 7 and 8 show the total DOS and local DOS for the substitutional Mn and donors in Ge and Si, respectively. Several important features emerge.

(1) Mn-doped Ge or Si are all half metals, regardless of the existence of donors such as As or P, which means the value of the total magnetic moment per Mn atom is integer.

(2) From the figures it can be determined that the moment per Mn is $3\mu_B$ in pure Ge or Si, and $4\mu_B$ after codoping with another donor. The importance of this finding, namely, codoping can actually increase the magnetic moment of Mn, will be discussed in the next subsection.

(3) The local DOS for Mn is broadened to the whole range of the host valence band, indicating that there is strong hybridization between the Mn $d$ state and the valence $p$ state of the host semiconductor.

(4) The local DOS of the donor is negligible, meaning that the states it contributes are mostly delocalized, so that its most evident influence on the total DOS is simply to shift the Fermi energy to a higher value, as is expected for a regular nonmagnetic dopant.

### B. Magnetic properties

At first sight, the introduced donors may negatively influence the strength of the magnetic interaction between Mn atoms, because of the compensation of hole carriers.[3,4,6] This argument may not be true for the following reason: We can write the magnetic interaction energy between two Mn ions as

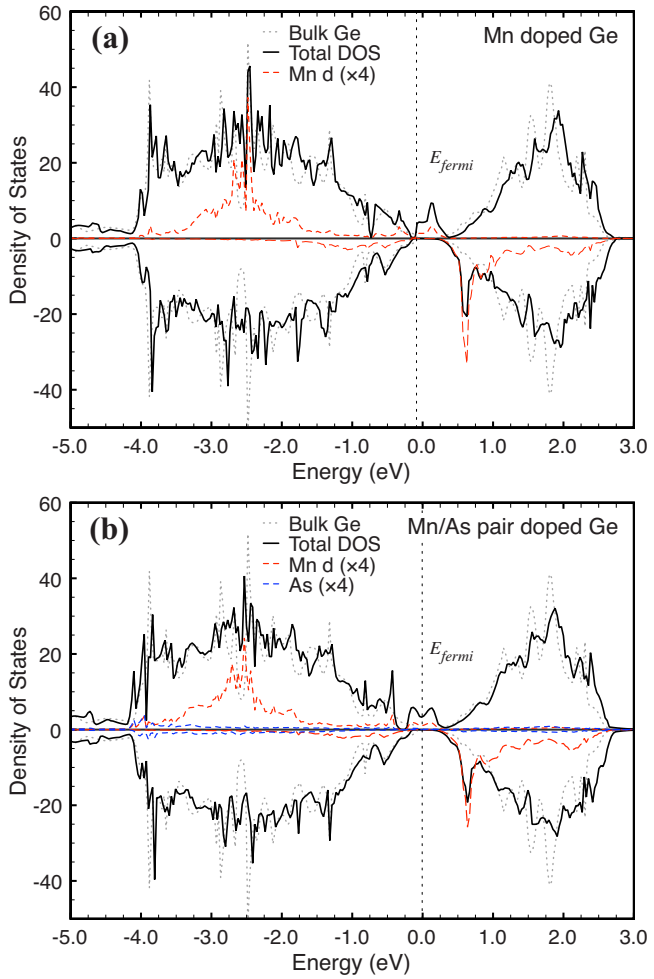


FIG. 7. (Color online) The spin-resolved DOS of (a) Mn-doped Ge and (b) a Mn/As pair-doped Ge. Projected DOS of Mn 3*d* states and As are given as red and blue dashed lines, respectively. The DOS for bulk Ge is shown for comparison.

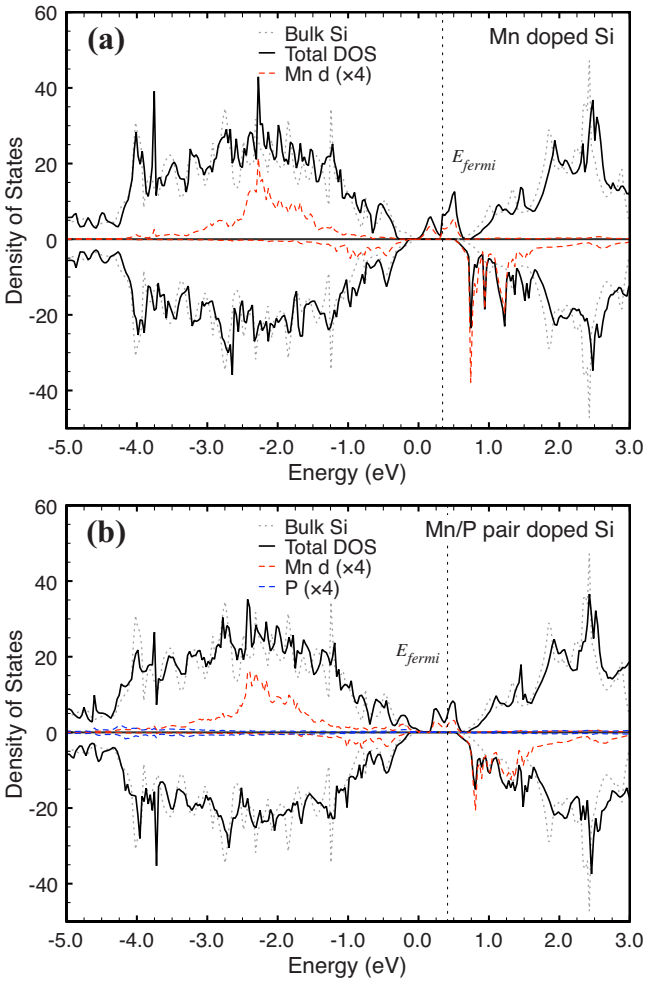


FIG. 8. (Color online) The spin-resolved DOS of (a) Mn-doped Si and (b) a Mn/P pair-doped Si. Projected DOS of Mn 3*d* states and P are given as red and blue dashed lines, respectively. The DOS for bulk Si is shown for comparison.

$$E_{\mathrm{Mn_1\text{-}Mn_2}} = J_{\mathrm{eff}} \mathbf{S}_{\mathrm{Mn_1}} \cdot \mathbf{S}_{\mathrm{Mn_2}}, \tag{3}$$

where $J_{\mathrm{eff}}$ denotes the effective magnetic coupling strength and $\mathbf{S}_{\mathrm{Mn_1}}$ and $\mathbf{S}_{\mathrm{Mn_2}}$ represent the local magnetic moments associated with the Mn atoms; even if $J_{\mathrm{eff}}$ were to decrease because of the carrier compensation effect, since the influence of the donor on the local moments of Mn is positive as mentioned in point (2) of the previous subsection, it is still possible that the enhancement of Mn moments by the donors outweighs its negative influence on $J_{\mathrm{eff}}$.

To check whether this is the case, we first resort to direct *ab initio* calculation of the magnetic coupling energy of a Mn-Mn pair with different separations, which can be represented by the total-energy difference $\Delta E$ between the antiferromagnetic (AFM) and the ferromagnetic (FM) states of the pair.[35–38] In the present case, each Mn atom has a donor neighbor, which leads to more spatial configurations with the same Mn-Mn distances. To be precise, a substitutional Mn atom has four nearest neighbors, that is, four possible sites for the donor atom, and thus there are 16 possible configurations for a given Mn-Mn distance. The number of nonequivalent configurations for each of 12 Mn-Mn separations in the range 2.4–9.5 Å in Si (2.5–10.0 Å in Ge) are 2, 6, 16, 4, 7, 16, 4, 7, 16, 10, 7, and 5, respectively, with increasing distance.

With these considerations, our results for Mn/As codoped Ge and Mn/P codoped Si are shown in Fig. 9. We first note that in the case of two Mn atoms in pure Ge [(a) and (b) of Fig. 9], the behavior of the AFM-FM energy difference $\Delta E$ is oscillatory between positive and negative values as a function of distance. In contrast, the average interaction between the two Mn/As pairs in Ge always favors FM coupling except at the nearest-neighbor Mn-Mn distance and this characteristics does not change with doping level [compare Fig. 9(a) of 3.125% Mn and Fig. 9(b) of 0.926% Mn]. In the case of Si as host [Fig. 9(c)], Mn atoms favor FM coupling except for nearest-neighbor distance and this feature does not change upon codoping.

Though usually it is assumed that the hole-mediated magnetic interaction in dilute magnetic semiconductors is Ruderman-Kittel-Kasuya-Yosida (RKKY) type, we find that the FM-AFM oscillation displayed in Fig. 9 should not be treated as a manifestation of the RKKY interaction.[35–38] Fig-

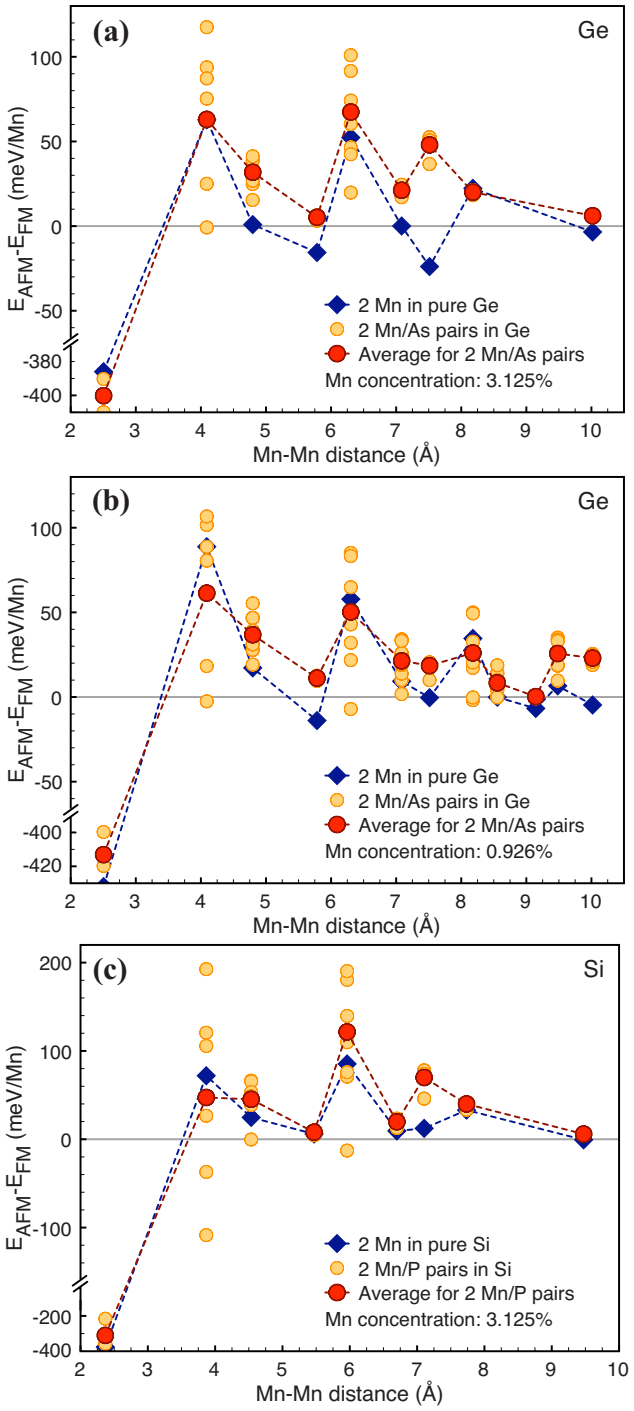


FIG. 9. (Color online) Total-energy difference between AFM and FM states of two Mn ions versus Mn-Mn separation for two Mn/As pairs-doped Ge at (a) 3.125% and (b) 0.939% Mn concentration; (c) for two Mn/P pairs-doped Si, represented by small orange dots. The large red dots are averages over the small orange dots for a given Mn-Mn distance. For comparison, the results for the systems doped with only two Mn impurities are shown as blue diamonds.

ure 10(a) shows the magnetic coupling between Mn ions along different lattice directions, which is similar to the design in work of Mahadevan *et al.*,[38] where it is evident that the oscillatory behavior is replaced by monotonic decrease.

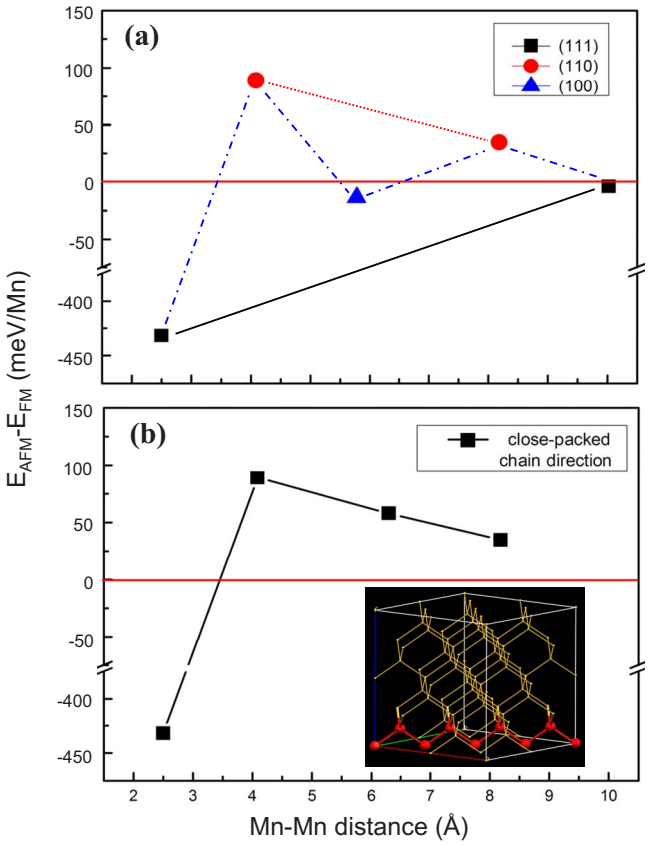


FIG. 10. (Color online) Magnetic coupling along (a) different lattice directions and (b) a close-packed chain, illustrated in the inset.

On the other hand, for the doping levels considered here, the period of RKKY oscillation is much larger than the lattice constant,[46,47] as in the case of GaAs. Thus, the oscillation here is merely due to magnetic anisotropy, rather than a manifestation of RKKY-type interaction. In Fig. 10(b), we plot the coupling along a close-packed atom chain, which also shows monotonic decrease with distance except for the nearest-neighbor value. Moreover, by comparing with Fig. 9(b), one can find that the magnetic coupling is strongest along this chain. This finding suggests that Mn ions in Ge are magnetically coupled through some paths consisting of covalently-bonded Ge atoms. A similar suggestion has been made for Mn-doped GaAs.[48]

There are two other important issues revealed in Fig. 9. First, the dispersive values of $\Delta E$ at a given distance in the codoped case show a different kind of magnetic anisotropy, which is caused by the relative positions of the two donors surrounding the magnetic impurities. This is different from the magnetic anisotropy typically discussed in the literature.[38,49] Second, in the presence of the donors, the FM interaction between two magnetic atoms on the whole preserves its magnitude rather than being substantially weakened. Thus, the influence of the donors on the magnetic properties of the whole system is not simply a weakening of the magnetic coupling by decreasing the number of interaction mediators.

Deeper understanding of the above observations requires a careful examination of the microscopic coupling mecha-

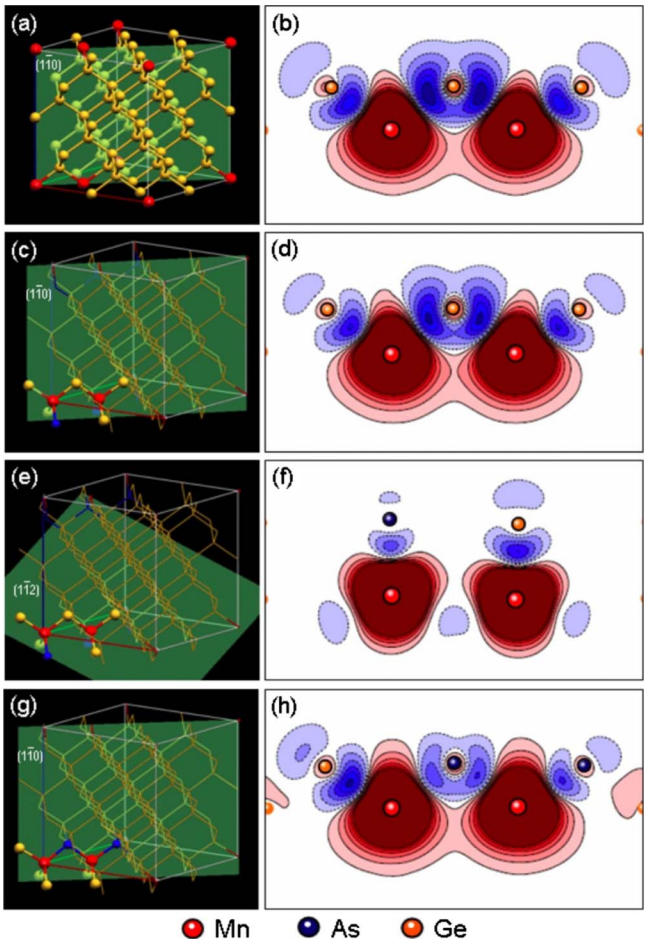


FIG. 11. (Color online) The atomic structures and spin density plots of three representative configurations of two Mn TOMS, (a) and (b), and two Mn/As pairs, (c)-(h), doped Ge. In all structures, the two Mn atoms are fixed at the next-nearest-neighbor distance. The spin density plots are taken on the green plane as depicted in the structures on the left. The red and blue contours represent the two different spin components. (c) and (e) correspond to the configuration with the strongest magnetic coupling between two Mn ions, and (g) the weakest magnetic coupling.

nism. To this end, we consider three representative configurations, all with the same Mn-Mn separation fixed, equal to the next-nearest-neighbor distance in the Ge matrix: (i) a Mn-Mn pair in pure Ge as the reference structure; (ii) and (iii) a Mn/As-Mn/As pair with the strongest and weakest magnetic couplings, respectively. For the reference case shown in Fig. 11(a), the two Mn atoms share a Ge atom as their nearest neighbor. When the two Mn atoms are ferromagnetically coupled, the spin density in the plane containing the two Mn atoms and their mutual Ge neighbor [the $(1\bar{1}0)$ plane indicated in Fig. 11(a)] is plotted in Fig. 11(b). The red (blue) area represents spin-up (down) density. The large local magnetic moments of Mn induce spin polarization on the nearby nonmagnetic Ge atoms, which are antiferromagnetically coupled with the Mn atoms.

The corresponding plots for case (ii) are shown in Figs. 11(c) and 11(d). In this case, the two As atoms are not in the $(1\bar{1}0)$ plane, and the two Mn atoms still have the same Ge atom as their mutual nearest neighbor. Furthermore, the local magnetic moment of the bridging Ge atom shows little change, indicating that $J_{\text{eff}}$ essentially stays the same. To show the effect of As doping, we plot in Fig. 11(f) the spin density on the plane containing the two Mn and one As atom [the $(1\bar{1}2)$ plane in Fig. 11(e)]. Here, As acts as a donor helping to compensate the holes introduced by its neighboring Mn, resulting in an increased local magnetic moment on each Mn atom, $S_{\text{Mn}}$ $(3.60\mu_B \rightarrow 4.00\mu_B)$. Therefore, the overall magnetic coupling between the two Mn atoms is enhanced relative to the pure Ge case.

For case (iii), the corresponding plots are shown in Figs. 11(g) and 11(h). In this case, the two As and two Mn atoms are both in the $(1\bar{1}0)$ plane, with one As replacing the mutual nearest Ge neighbor of the two Mn atoms. Similar to case (ii), here both $S_{\text{Mn1}}$ and $S_{\text{Mn2}}$ are also increased—$S_{\text{Mn1}}$: $3.60\mu_B \rightarrow 3.87\mu_B$; $S_{\text{Mn2}}$: $3.60\mu_B \rightarrow 4.02\mu_B$; the asymmetry in the increase is caused by the asymmetric locations of the two As atoms. However, because the local magnetic moment of the bridging atom is substantially decreased from that of case (i) (Ge: $-0.16\mu_B \rightarrow$ As: $-0.05\mu_B$), the corresponding $J_{\text{eff}}$ is also significantly weakened, leading to an overall weakened magnetic coupling between the two Mn atoms relative to the pure Ge case.

In summary, As as a donor can enhance the local magnetic moments of neighboring Mn atoms, but itself is weakly spin polarized (much weaker than Ge). Therefore, if As serves as the bridging atom between two Mn atoms, the global magnetic coupling will be weakened. If As is located so as to only enhance the magnetic moment of Mn, with a Ge atom still bridging the Mn-Mn coupling, then the global magnetic coupling will be enhanced. This conclusion is further confirmed by checking other Mn-Mn distances.

## V. CURIE TEMPERATURE

To study the macroscopic magnetic properties of the codoped DMS materials using our *ab initio* results, we turn to the classical Heisenberg model,

$$H = -\sum_{i,j} J_{ij}\sigma_i \cdot \sigma_j, \tag{4}$$

where $J_{ij}$ is the magnetic coupling constant between moment $i$ and $j$, and $\sigma_i$ is a unit vector representing the direction of spin $i$. Then the AFM-FM energy difference $\Delta E$ calculated in previous section is given by

$$\Delta E = E_{\text{AFM}} - E_{\text{FM}} = 4J_{12}, \tag{5}$$

with 1 and 2 as the indices of the two moments in the supercell. With given coupling parameters, we then use Monte Carlo simulations to address the statistical mechanics of the DMS systems at finite temperatures. To eliminate finite-size effects, the cumulant crossing method[40,41] is used to determine the Curie temperature. This two-step approach has the distinct advantage over the ordinary mean-field approach, both disorder and percolation effects are naturally and precisely taken into account.[50,51]

A subtle issue in the present case is the following. Since real interactions between magnetic atoms in DMS have a

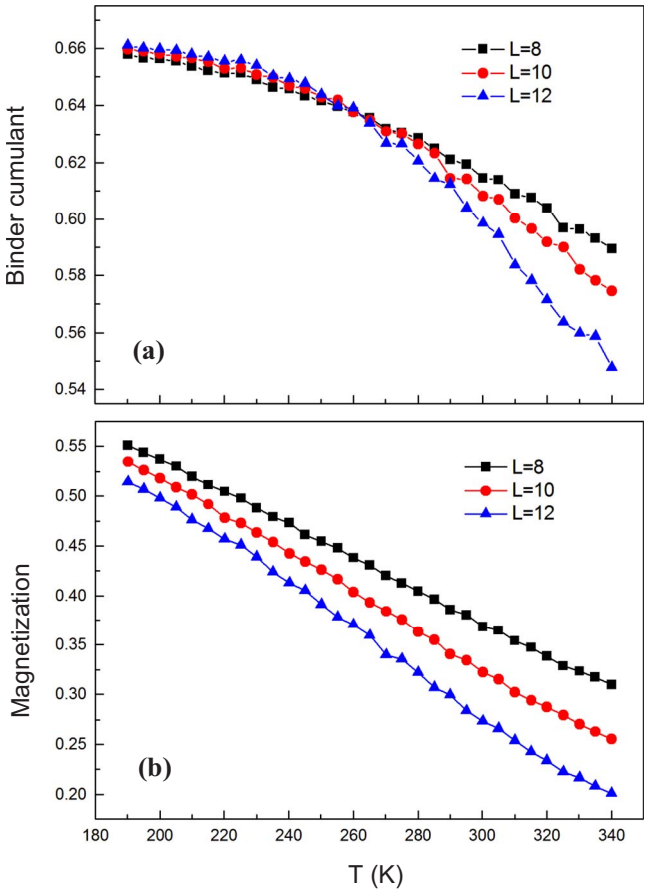


FIG. 12. (Color online) Monte Carlo results of (a) Binder cumulant and (b) normalized magnetization of 5% Mn/As codoped Ge.

built-in multiatom nature, in an optimal Heisenberg description the coupling parameters must depend on the system geometry. This is difficult, if not entirely impossible[52,53] to address, because of the very large number of possible configurations in a macroscopic system and some approximations are necessary.

The supercell *ab initio* approach[48,54–57] employed here assumes the pair-superposition approximation, which means that the interaction is exclusively pairwise and can be added independently to get the total interaction. Though this may not hold at high concentrations of magnetic moments, we claim that it should be a reasonable approximation at the low concentrations we considered (3.13 %–6 %), where the average distance between two Mn atoms, estimated by

$$\bar{d} = 2\sqrt[3]{\frac{3}{32\pi x}}a, \tag{6}$$

with $x$ as the concentration and $a$ as the lattice constant, which ranges from $1.97a$ to $1.58a$ or 11.39 to 9.14 Å in the case of Mn doped Ge. Considering the bond length $d_{\text{bond}}$ in Ge is only about 2.5 Å, a separation $\sim 4d_{\text{bond}}$ is large enough for the system to be treated in this approximation.

We use three supercell sizes, $8\times8\times8$, $10\times10\times10$, and $12\times12\times12$, where the unit length is the edge length of a fcc

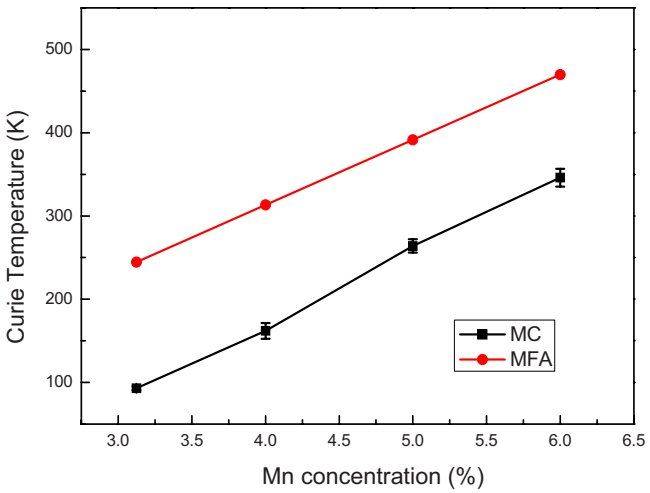


FIG. 13. (Color online) Comparison between Curie temperatures calculated by the Monte Carlo approach (MC, black squares) and those obtained by the mean-field approximation (MFA, red dots).

cube. The number of spin in a supercell is calculated by $x8L^3$, where $x$ is the spin concentration. Take the case of $x=5\%$ as an example, we have 205, 400, and 691 spins, respectively, in the three corresponding supercells. In our simulations these numbers are large enough to give a reliable result of $T_c$. The Binder cumulant data and normalized magnetization of 5% Mn/As codoped Ge are shown in Fig. 12 as an example. For disorder averaging in evaluating the Curie temperature, we use 40 randomly generated spin configurations for each supercell size. To check the accuracy we also increase the number of configurations to 100 and no obvious deviations are detected.

Using the *ab initio* coupling parameters for $Mn_xGe_{1-x}$, we first find that MC does not yield identifiable $T_c$ up to $x=6\%$ (see below). Nevertheless, after codoping with As, MC shows that the system has high $T_c$, as summarized in Fig. 13, in which we also include the results from the mean-field approximation (MFA) using the formula[58]

$$T_c = \frac{1}{k_B}\frac{2x}{3}\sum_{i\neq 0} J_{0i}. \tag{7}$$

These results show that the MFA greatly overestimates the Curie temperature, as established before.[50,51,58] At $x=5\%$, $T_c$ is evaluated to be 264 K through MC, which is much higher than the 118 K of 5% Mn-doped GaAs.[59] At the 6% Mn concentration, MC gives a $T_c$ higher than room temperature. Considering that $x=6\%$ is already a relatively high concentration, we expect that the pair-superposition approximation may not be valid in this case. Arsenic doping can still be expected to dramatically change the magnetic properties of Mn-doped Ge, namely, from no finite $T_c$ to a potentially high-$T_c$ DMS material.

The dependence of the Curie temperature on Mn concentration, as obtained from the MC results, is almost linear. This behavior is partly due to the pair-superposition approximation we used, meaning that the strength of magnetic cou-

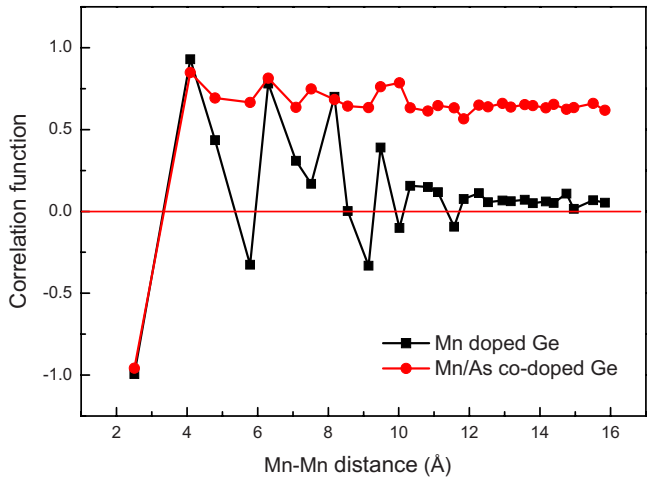


FIG. 14. (Color online) Spin-spin correlation function obtained from the Monte Carlo simulations.

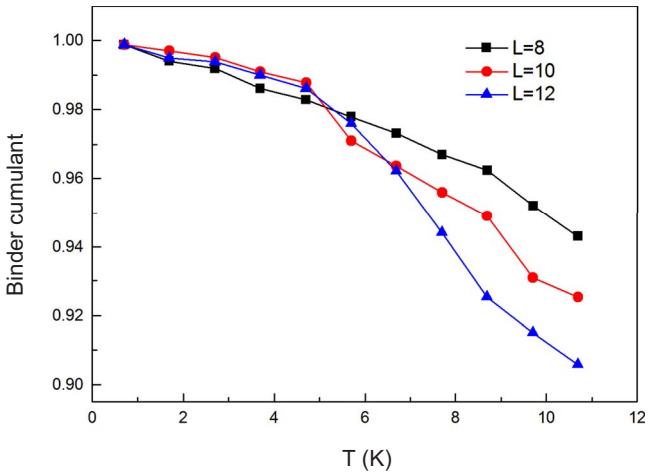


FIG. 15. (Color online) Spin-glass Binder cumulant of 5% Mn doped Ge.

pling does not depend on Mn concentration. The only influence of concentration on $T_c$ is the average number of magnetic impurity atoms on each coordination shell. Thus, after the configurational average, we expect that the dependence of $T_c$ on $x$ resembles the linear one obtained within the MFA [Eq. (7)]. Another reason for this linearity is that the concentrations we studied are higher than the magnetic percolation threshold of this system.[58]

The presence of AFM couplings and the absence of $T_c$ in the case of pure Mn-doped Ge suggests the possibility of a spin-glass ground state for this system. Jaeger *et al.*[60] claimed that at low-temperature $Mn_xGe_{1-x}$ exhibits spin-glass-like behavior and the critical temperature of the spin-glass phase transition is 12 and 15 K, for Mn concentrations $x=0.04$ and $x=0.2$, respectively. To examine whether this is the case, we first study the spin-spin correlation function of 5% Mn-doped Ge, at $T=0.01K$. The result is shown in Fig. 14, along with a plot for Mn/As codoped Ge, for comparison. The correlation function of $Mn_xGe_{1-x}$ decays very fast with increasing distance and approaches to zero, indicating the absence of FM order even at low temperatures. We then use the Edwards-Anderson spin-glass order parameter,[61] defined as

$$q = [\langle \mathbf{S}_i \rangle_T^2]_{av}, \tag{8}$$

and calculate the spin-glass cumulant of 5% Mn-doped Ge using the two-replica algorithm developed by Bhatt and Young.[62] After averaging over 100–200 configurations for each supercell size, our Monte Carlo simulations yield a transition temperature ~5 K (Fig. 15), a value in semiquantitative agreement with the results of Jaeger *et al.*[60]

## VI. DISCUSSION

$Mn_xGe_{1-x}$ has been attractive within the DMS community because of its easy incorporation into the current semiconductor industry. The mechanism of valence hole-mediated ferromagnetism for (Ga,Mn)As was proposed years ago[4,46,63] and has been extensively accepted ever since, but there is still no definitive theory for $Mn_xGe_{1-x}$.[6] One reason, which is also one of the main points of this paper, is the difficulty of decreasing the percentage of interstitial Mn dopants. The other important point is the hard-to-control inhomogeneity of this system, which has been realized only in recent years. The high Curie temperature formerly reported in $Mn_xGe_{1-x}$ (Refs. 9 and 64) is now thought to be due to the formation of Mn-rich regions in the host semiconductor.[6,33,60,65,66] For example, Mn-rich nanodots[67] and nanocolumns[24,68,69] in $Mn_xGe_{1-x}$ have been reported by many experimental groups and later reproduced in Monte Carlo simulations.[70]

Despite the seemingly unavoidable precipitation or spinodal decomposition[66] present during the growth of $Mn_xGe_{1-x}$ samples, the study on homogeneously-doped $Mn_xGe_{1-x}$ has never stopped. Work by Li *et al.*[33,65] indicates that the long-range FM order in $Mn_xGe_{1-x}$ only exists at low temperatures ($\leq$12 K). Jaeger *et al.*[60] claimed that even at low temperatures $Mn_xGe_{1-x}$ shows spin-glass-type behavior, and proposed that this is due to the intercluster frustration between FM Mn-rich clusters. Recently, Zeng *et al.*,[15] using a newly developed subsurfactant epitaxy method, successfully grew cluster-free $Mn_xGe_{1-x}$ samples with a Mn doping level of 0.25%. Surprisingly, this low doping level (by normal DMS standards, where 1% to 5% is typical) led to a Curie temperature as high as over 400 K.

The results in the present work provide a viewpoint that may resolve the seemingly conflicting experimental results discussed above. Specifically, we showed that the magnetic coupling between Mn ions in $Mn_xGe_{1-x}$ oscillates between FM and AFM with increasing Mn-Mn distance and that homogeneous $Mn_xGe_{1-x}$ exhibits spin-glass behavior. Thus, the FM order observed in experiments could be due to spatially ordered structures, which are formed due to precipitation or spinodal decomposition. The high-transition temperatures are expected because of the large concentration of magnetic moments within the clusters. On the other hand, the AFM frustration in this case only manifest itself in the intercluster interaction, and thus leads to the spin-glass behavior at low temperatures.

The unexpected high $T_c$ in Zeng's work requires more discussion. Upon codoping with donor As, the AFM cou-

pling between Mn ions is absent, and a high-Curie temperature emerges. We thus speculate that the high-transition temperature in this case originates from this codoping effect, and the unexpected donor here is most probably oxygen. Indeed, a recent study on the role of oxygen defects in $Mn_xGe_{1-x}$ by Continenza and Profeta[71] supports this scenario, namely, that oxygen acts as an *n*-type codopant and facilitates the substitutional Mn doping. It is also reasonable to expect a positive influence of oxygen on the Mn-Mn magnetic coupling, which, together with the possible existence of Mn-rich regions, can lead to a high-Curie temperature.

Recently, the works of Kuroda *et al.*[72] and Bonanni *et al.*[73] demonstrated experimentally that the aggregation of magnetic ions in DMS systems can be controlled by modifying the charge states of the magnetic dopants. This is in agreement with the spirit of our work, that is, charge states of impurity dopants play an important role in the growth kinetics of DMS materials and can lead to different structures with their own specific properties.

Finally, this work suggests that the enhancement of substitutional Mn concentration in group-IV DMS can be achieved in epitaxial growth by codepositing with the donors. More specifically, this codoping method can be integrated in the recently developed subsurfactant epitaxial growth,[15] where pure Ge layers epitaxially grow on a Ge(100) substrate precovered with a submonolayer of Mn. During the growth process, the Mn atoms tend to diffuse upward to the subsurface layer, as predicted in a previous theoretical study.[74] When the growth is slow enough, a small fraction of the Mn atoms can be trapped in substitutional sites, which leads to homogeneous substitutional Mn doping with all the interstitial Mn floating at the subsurface layer. However, the resulting Mn concentration is still pretty low (0.25%). Here we propose that by codepositing Ge with another donor, with very low depositing rates, the growth front could mimic the subsurfactant growth mode, but with more efficient substitutional trapping of Mn. The Mn trapping rate can be controlled by changing the concentration of the donor. Experimental confirmation of this codoping scheme is highly desirable.

## VII. CONCLUSION

In conclusion, our *ab initio* DFT calculations show that in DMS materials *n*-type electronic codopants (donors) can serve to enhance the substitutional doping of *p*-type magnetic dopants such as Mn in the host group-IV semiconductors Si and Ge. The donors suppress to a large extent the charge and magnetic-moment compensating effects from interstitial Mn, which is detrimental to FM order. We calculate the magnetic coupling between moments associated with Mn atoms using the energy difference between parallel and antiparallel aligned pairs of Mn moments. We examined the unconventional magnetic anisotropy in Mn/As codoped Ge, namely, the dependence of magnetic coupling on the relative positions of magnetic ions and their neighboring donors. We find that the coupling oscillates between FM and AFM with increasnig Mn-Mn distance in the Mn-doped Ge, whereas in As/Mn *n-p* codoped Ge the coupling values at Mn-Mn separations up to the 12th coordination shell are all FM, except for the nearest-neighbor one. We find that the FM-AFM oscillatory behavior in $Mn_xGe_{1-x}$ is due to anisotropy rather than being the result of a RKKY-type interaction. The magnitude of Mn-Mn ferromagnetic couplings is also enhanced upon codoping with donors. By studying the local spin density around the Mn and As dopants, we find As donors can increase the local magnetic moments on the Mn. Therefore, despite the carrier compensation by the donors, the ferromagnetic interaction between the Mn ions, and accordingly, the Curie temperature, can still be enhanced. Our Monte Carlo simulations, using magnetic coupling parameters obtained from the *ab initio* calculations, indicate a high Curie temperature in Mn/As-Ge of 264 K at 5% Mn doping. On the other hand, no FM order is observed in $Mn_xGe_{1-x}$ (without codoping) as Mn concentration ranges from 3.13% to 6%. Thus, the homogeneously doped $Mn_xGe_{1-x}$ is most likely a generic spin glass, with a spin-glass transition temperature of 5 K at 5% doping, also obtained from our Monte Carlo simulations. Accordingly, we suggest that the high Curie temperature observed experimentally in $Mn_xGe_{1-x}$ is either due to the formation of Mn-rich spatially ordered regions or to *n-p* codoping effects from the *n*-type oxygen impurities, or a combination of both.

## ACKNOWLEDGMENTS

The authors thank Adriana Moreo, Rong Yu, and Shuai Dong for helpful discussions and Kirk H. Bevan for a critical reading of the paper. This work was supported in part by NSF under Grant Nos. DMR-0325218 and DMR-0606485, by DOE under Grant No. DE-FG02-05ER46209, and in part by the Division of Materials Sciences and Engineering, Office of Basic Energy Sciences, DOE. The calculations were performed at NERSC of DOE and NCCS of ORNL.

[1] S. A. Wolf, D. D. Awschalom, R. A. Buhrman, J. M. Daughton, S. von Molnár, M. L. Roukes, A. Y. Chtchelkanova, and D. M. Treger, Science **294**, 1488 (2001).

[2] I. Žutić, J. Fabian, and S. Das Sarma, Rev. Mod. Phys. **76**, 323 (2004).

[3] H. Ohno, Science **281**, 951 (1998).

[4] T. Dietl, H. Ohno, F. Matsukura, J. Cibert, and D. Ferrand, Science **287**, 1019 (2000).

[5] R. N. Bhatt, M. Berciu, M. P. Kennett, and X. Wan, J. Supercond. **15**, 71 (2002).

[6] T. Jungwirth, J. Sinova, J. Mašek, J. Kučera, and A. H. MacDonald, Rev. Mod. Phys. **78**, 809 (2006).

[7] C. Timm, J. Phys.: Condens. Matter **15**, R1865 (2003).

[8] S. Sanvito, G. Theurich, and N. A. Hill, J. Supercond. **15**, 85

(2002).
[9] Y. D. Park, A. T. Hanbicki, S. C. Erwin, C. S. Hellberg, J. M. Sullivan, J. E. Mattson, T. F. Ambrose, A. Wilson, G. Spanos, and B. T. Jonker, Science **295**, 651 (2002).
[10] H. Ohta, S. Okubo, J. Yoshikawa, Y. Nakashima, C. Urakawa, H. Nakayama, and T. Nishino, Physica B **298**, 449 (2001).
[11] H. Nakayama, H. Ohta, and E. Kulatov, Physica B **302**, 419 (2001).
[12] S. Abe, Y. Nakasima, S. Okubo, H. Nakayama, T. Nishino, H. Yanagi, H. Ohta, and S. Iida, Appl. Surf. Sci. **142**, 537 (1999).
[13] M. Bolduc, C. Awo-Affouda, A. Stollenwerk, M. B. Huang, F. G. Ramos, G. Agnello, and V. P. LaBella, Phys. Rev. B **71**, 033302 (2005).
[14] S. Picozzi, F. Antoniella, and A. Continenza, A. MoscaConte, A. Debernardi, and M. Peressi, Phys. Rev. B **70**, 165205 (2004).
[15] C. Zeng, Z. Y. Zhang, K. van Benthem, M. F. Chisholm, and H. H. Weitering, Phys. Rev. Lett. **100**, 066101 (2008).
[16] S. C. Erwin and A. G. Petukhov, Phys. Rev. Lett. **89**, 227201 (2002).
[17] R. Wu, Phys. Rev. Lett. **94**, 207201 (2005).
[18] S. Hao and Z. Y. Zhang, Phys. Rev. Lett. **99**, 166101 (2007).
[19] K. M. Yu, W. Walukiewicz, T. Wojtowicz, I. Kuryliszyn, X. Liu, Y. Sasaki, and J. K. Furdyna, Phys. Rev. B **65**, 201303(R) (2002).
[20] K. C. Ku, S. J. Potashnik, R. F. Wang, S. H. Chun, P. Schiffer, N. Samarth, M. J. Seong, A. Mascarenhas, E. Johnston-Halperin, R. C. Myers, A. C. Gossard, and D. D. Awschalom, Appl. Phys. Lett. **82**, 2302 (2003).
[21] K. W. Edmonds, P. Bogusławski, K. Y. Wang, R. P. Campion, S. N. Novikov, N. R. S. Farley, B. L. Gallagher, C. T. Foxon, M. Sawicki, T. Dietl, M. Buongiorno Nardelli, and J. Bernholc, Phys. Rev. Lett. **92**, 037201 (2004).
[22] F. D'Orazio, F. Lucari, S. Santucci, P. Picozzi, A. Verna, M. Passacantando, N. Pinto, L. Morresi, R. Gunnella, and R. Murri, J. Magn. Magn. Mater. **262**, 158 (2003).
[23] C. G. Zeng, W. Zhu, S. C. Erwin, Z. Y. Zhang, and H. H. Weitering, Phys. Rev. B **70**, 205340 (2004).
[24] M. Jamet, A. Barski, T. Devillers, V. Poydenot, R. Dujardin, P. Bayle-Guillmaud, J. Rotheman, E. Bellet-Amalric, A. Marty, J. Cibert, R. Mattana, and S. Tatarenko, Nature Mater. **5**, 653 (2006).
[25] Y. H. Kwon, T. W. Kang, H. Y. Cho, and T. W. Kim, Solid State Commun. **136**, 257 (2005).
[26] W. G. Zhu, Z. Y. Zhang, and E. Kaxiras, Phys. Rev. Lett. **100**, 027205 (2008).
[27] G. Kresse and J. Furthmüller, Phys. Rev. B **54**, 11169 (1996).
[28] P. E. Blöchl, Phys. Rev. B **50**, 17953 (1994).
[29] G. Kresse and D. Joubert, Phys. Rev. B **59**, 1758 (1999).
[30] J. P. Perdew, K. Burke, and M. Ernzerhof, Phys. Rev. Lett. **77**, 3865 (1996).
[31] C. R. Hubbard, H. E. Swanson, and F. A. Mauer, J. Appl. Crystallogr. **8**, 45 (1975).
[32] H. P. Singh, Acta Crystallogr. **A24**, 469 (1968).
[33] A. P. Li, J. Shen, J. R. Thompson, and H. H. Weitering, Appl. Phys. Lett. **86**, 152507 (2005).
[34] S. B. Ma, Y. P. Sun, B. C. Zhao, P. Tong, X. B. Zhu, and W. H. Song, Solid State Commun. **140**, 192 (2006).
[35] Y.-J. Zhao, T. Shishidou, and A. J. Freeman, Phys. Rev. Lett. **90**, 047204 (2003).
[36] A. Stroppa, S. Picozzi, A. Continenza, and A. J. Freeman, Phys. Rev. B **68**, 155203 (2003).
[37] H. Weng and J. Dong, Phys. Rev. B **71**, 035201 (2005).
[38] P. Mahadevan, A. Zunger, and D. D. Sarma, Phys. Rev. Lett. **93**, 177201 (2004).
[39] G. Henkelman, B. P. Uberuaga, and H. Jónsson, J. Chem. Phys. **113**, 9901 (2000).
[40] K. Binder, Phys. Rev. Lett. **47**, 693 (1981).
[41] K. Binder and D. W. Heermann, *Monte Carlo Simulation in Statistical Physics* (Springer, Berlin, 2002).
[42] H. Ohno, A. Shen, F. Matsukura, A. Oiwa, A. Endo, S. Katsumoto, and Y. Iye, Appl. Phys. Lett. **69**, 363 (1996).
[43] H. Ohno, F. Matsukura, T. Omiya, and N. Akiba, J. Appl. Phys. **85**, 4277 (1999).
[44] A. J. R. da Silva, A. Fazzio, and A. Antonelli, Phys. Rev. B **70**, 193205 (2004).
[45] S. Picozzi, M. Ležaić, and S. Blügel, Phys. Status Solidi A **203**, 2738 (2006).
[46] F. Matsukura, H. Ohno, A. Shen, and Y. Sugawara, Phys. Rev. B **57**, R2037 (1998).
[47] J. Kudrnovský, I. Turek, V. Drchal, F. Máca, P. Weinberger, and P. Bruno, Phys. Rev. B **69**, 115208 (2004).
[48] L. M. Sandratskii and P. Bruno, Phys. Rev. B **67**, 214402 (2003).
[49] D. S. Wang, R. Wu, and A. J. Freeman, Phys. Rev. Lett. **70**, 869 (1993).
[50] K. Sato, W. Schweika, P. H. Dederichs, and H. Katayama-Yoshida, Phys. Rev. B **70**, 201202(R) (2004).
[51] L. Bergqvist, O. Eriksson, J. Kudrnovský, V. Drchal, P. A. Korzhavyi, and I. Turek, Phys. Rev. Lett. **93**, 137202 (2004).
[52] A. Franceschetti, S. V. Dudiy, S. V. Barabash, A. Zunger, J. Xu, and M. van Schilfgaarde, Phys. Rev. Lett. **97**, 047202 (2006).
[53] A. Franceschetti, A. Zunger, and M. van Schilfgaarde, J. Phys.: Condens. Matter **19**, 242203 (2007).
[54] S. Sanvito and N. A. Hill, Appl. Phys. Lett. **78**, 3493 (2001).
[55] A. J. R. da Silva, A. Fazzio, R. R. dos Santos, and L. E. Oliveira, J. Phys.: Condens. Matter **16**, 8243 (2004).
[56] M. Wierzbowska, D. Sánchez-Portal, and S. Sanvito, Phys. Rev. B **70**, 235209 (2004).
[57] S. Picozzi and M. Ležaić, New J. Phys. **10**, 055017 (2008).
[58] L. Bergqvist, O. Eriksson, J. Kudrnovský, V. Drchal, A. Bergman, L. Nordström, and I. Turek, Phys. Rev. B **72**, 195210 (2005).
[59] K. W. Edmonds, K. Y. Wang, R. P. Campion, A. C. Neumann, N. R. S. Farley, B. L. Gallagher, and C. T. Foxon, Appl. Phys. Lett. **81**, 4991 (2002).
[60] C. Jaeger, C. Bihler, T. Vallaitis, S. T. B. Goennenwein, M. Opel, R. Gross, and M. S. Brandt, Phys. Rev. B **74**, 045330 (2006).
[61] S. F. Edwards and P. W. Anderson, J. Phys. F: Met Phys **5**, 965 (1975).
[62] R. N. Bhatt and A. P. Young, Phys. Rev. B **37**, 5606 (1988).
[63] H. Ohno, J. Magn. Magn. Mater. **200**, 110 (1999).
[64] S. Cho, S. Choi, S. C. Hong, Y. Kim, J. B. Ketterson, B.-J. Kim, Y. C. Kim, and J.-H. Jung, Phys. Rev. B **66**, 033303 (2002).
[65] A. P. Li, J. F. Wendelken, J. Shen, L. C. Feldman, J. R. Thompson, and H. H. Weitering, Phys. Rev. B **72**, 195205 (2005).
[66] T. Dietl, J. Appl. Phys. **103**, 07D111 (2008).
[67] D. Bougeard, S. Ahlers, A. Trampert, N. Sircar, and G. Abstreiter, Phys. Rev. Lett. **97**, 237202 (2006).
[68] J.-S. Kang, G. Kim, S. C. Wi, S. S. Lee, S. Choi, Sunglae Cho, S. W. Han, K. H. Kim, H. J. Song, H. J. Shin, A. Sekiyama, S. Kasai, S. Suga, and B. I. Min, Phys. Rev. Lett. **94**, 147202

(2005).
[69] A. P. Li, C. Zeng, K. van Benthem, M. F. Chisholm, J. Shen, S. V. S. Nageswara Rao, S. K. Dixit, L. C. Feldman, A. G. Petukhov, M. Foygel, and H. H. Weitering, Phys. Rev. B **75**, 201201(R) (2007).
[70] H. Katayama-Yoshida, K. Sato, T. Fukushima, M. Toyoda, H. Kizaki, V. A. Dinh, and P. H. Dederichs, Phys. Status Solidi A **204**, 15 (2007).
[71] A. Continenza and G. Profeta, Phys. Rev. B **78**, 085215 (2008).
[72] S. Kuroda, N. Nishizawa, K. Takita, M. Mitome, Y. Bando, K. Osuch, and T. Dietl, Nature Mater. **6**, 440 (2007).
[73] A. Bonanni, A. Navarro-Quezada, T. Li, M. Wegscheider, Z. Matěj, V. Holý, R. T. Lechner, G. Bauer, M. Rovezzi, F. D'Acapito, M. Kiecana, M. Sawicki, and T. Dietl, Phys. Rev. Lett. **101**, 135502 (2008).
[74] W. G. Zhu, H. H. Weitering, E. G. Wang, E. Kaxiras, and Z. Y. Zhang, Phys. Rev. Lett. **93**, 126102 (2004).